www.czasopisma.pan.pl PAN POLSKA AKADEMIA NAUK www.journals.pan.pl

Arch. Metall. Mater. **67** (2022), 2, 787-796

DOI: https://doi.org/10.24425/amm.2022.137819

BIAO-HUA QUE[1], LU WANG[1,3*], BAO WANG[2*], YI CHEN[2], ZHENG-LIANG XUE[2]

INFLUENCE OF NaCl ADDITIVE ON THE REDUCTION PROCESS OF MoO_3 TO Mo_2C BY HIGH-PURITY CO GAS

In this work, influence of NaCl additive on the transformation process of MoO_3 to Mo_2C under pure CO atmosphere in the range of room temperature to 1170 K was investigated. The results showed that transformation of MoO_3 to Mo_2C can be roughly divided into two stages: the reduction of MoO_3 to MoO_2 (the first stage) and the carburization of MoO_2 to Mo_2C (the second stage). As to the first stage, it was found that increasing the content of NaCl (from 0 to 0.5 wt.%) was beneficial for the increase of reaction rate due to the nucleation effect; while when the content of NaCl increased to 2 wt.%, the reaction rate will be decreased in turn. As to the second stage, the results showed that reaction rate was decreased with the increase of NaCl, which may be due to the formation of low-melting point eutectic. The work also found that morphology of as-prepared Mo_2C was irregular and particle size of it was gradually increased with increasing the NaCl content. According to the results, the possible reaction mechanism was proposed.

Keywords: Mo_2C;·MoO_3; CO;·NaCl

1. Introduction

As a new functional material, molybdenum carbide (Mo_2C) has many superior properties such as thermal stability, high elastic modulus, high melting point, high hardness, wear resistance, and good corrosion resistance [1-2]. What is more, Mo_2C has been found to have excellent catalytic properties, especially in hydrogen-involved reactions such as hydrogenation reaction [3-4], hydro-desulfurization (HDS) [5], hydrogenation deoxygenation [6], and hydro-denitrogenation (HDN) [7-8]. Therefore, the preparation of Mo_2C has attracted increasing attention and many methods have been reported in recent years, such as gas reduction (carburization of MoO_3 with mixed C_4H_{10}/H_2 [9] or CO/CO_2 gases [10-11], carbonization of MoO_2 with CH_3OH [12] or CO gas [13]), alkalide reduction [14], and sonochemical synthesis [15].

Recently, salt has been used as an assistance in various preparation methods. During the salt melt synthesis method (SMS), as a high-temperature ionic melt, salt melt can provide strong polarizing force and possessed the advantage of easy isolation from the product, which offers unparalleled solvation power for oxides and covalent [16]. They have been widely used as reaction media for inorganic materials, including oxide ceramic [17], non-oxides [18], semiconductors [19], and carbon nanostructures [20]. With the aspect of chemical vapor deposition method (CVD), the addition of a certain of salt could play an important role on lowering the melting point of precursors, increasing their vapor pressure, and decreasing the activation energy [21], which enables the synthesis of various 2D materials, such as transition metal chalcogenides (TMCs) [22], non-layered compounds [23], perovskites [24] and heterostructures [25].

What is more, salts were also widely used in the shaped-controlled synthesis of metallic molybdenum and its compounds. For example, it was found that the use of the alkali metal carbonates (Na_2CO_3, Li_2CO_3, and K_2CO_3) [26] and chlorate additives (NaCl, KCl, and $CaCl_2$) [27-28] could control the shape and refine the particles size of prepared product during the reduction of molybdenum oxides with H_2. However, relative studies for the preparation of Mo_2C were still lacking. To make up this gap, the present work was initiated. Among these salts, NaCl was very common and convenient, it also has been considered as one of the representative salts, so in this work NaCl was

[1] WUHAN UNIVERSITY OF SCIENCE AND TECHNOLOGY, HUBEI PROVINCIAL KEY LABORATORY FOR NEW PROCESSES OF IRONMAKING AND STEELMAKING, WUHAN 430081, CHINA
[2] WUHAN UNIVERSITY OF SCIENCE AND TECHNOLOGY, THE STATE KEY LABORATORY OF REFRACTORIES AND METALLURGY, WUHAN 430081, CHINA
[3] FOSHAN (SOUTHERN CHINA) INSTITUTE FOR NEW MATERIALS, FOSHAN 528200, GUANGDONG, CHINA

* Corresponding authors: wanglu@wust.edu.cn; wangbao1983@wust.edu.cn

chosen as the additive for the experimental purposes. Influence of various contents of additive (0, 0.1, 0.5, and 2 wt.% NaCl) on the reaction rate, morphology evolution, and particle size of the as-prepared Mo_2C during the reduction process of MoO_3 to Mo_2C by CO gas were illustrated.

2. Materials and experimental procedures

2.1. Materials

High-purity (99.95 wt.%) MoO_3 from Shanghai Aladdln Biochemical Technology Co., Ltd. were used as the experimental raw materials. From its XRD pattern and scanning electronic micrograph (SEM), as shown in Figs. 1 and 2, respectively, it can be known that the main peaks are in well consistent with MoO_3 (PDF card No. 5-508) and the powders are composed of many small platelet-shaped particles with fairly dense structure.

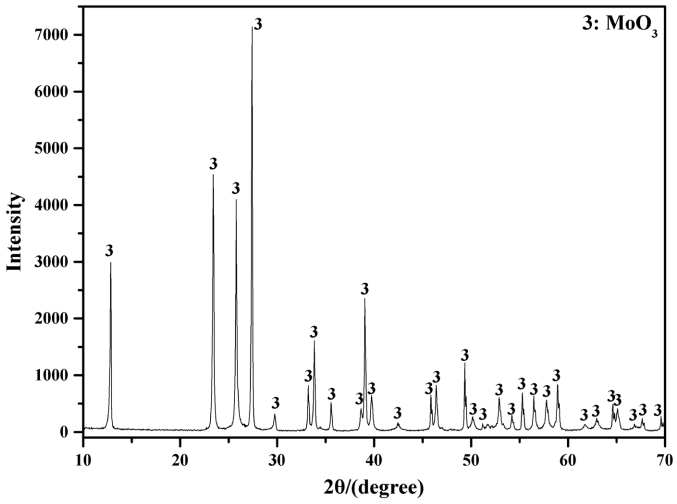

Fig. 1. XRD pattern of raw material MoO_3

2.2. Experimental procedures

In order to investigate the influence of NaCl additive on the reaction behavior of MoO_3 to Mo_2C, pure 5 g MoO_3 powders (defined as the mixed samples with 0 wt.% NaCl additive) and MoO_3 samples mixed with different concentrations of NaCl (0.1, 0.5, and 2 wt.%, which were prepared by the spraying method) were used as the experimental raw materials.

The weight change of samples during the reduction process was monitored by the thermogravimetric analyzer (HCT-3, Beijing Hengjiu, Instrument Ltd., China), the corresponding experimental setup is shown in Fig. 3. In each experimental run, a mixture of sample about 65 mg was used and put into the furnace after loading it into the alumina crucible "6". High-purity argon was first introduced to flush air out of the furnace. Then the furnace was heated from room temperature to 1170 K at the heating rate of 10 K/min under pure CO gas atmosphere. After the experiment was completed, CO gas was switched to Ar gas again and then the product was cooled down to room temperature. To gain insight into the reaction processes of MoO_3 to Mo_2C, products obtained at different reaction extents were also prepared in the case of 2 wt.% NaCl-doped mixtures. All of the products obtained at different conditions were collected for the further detection.

In all the experimental runs, a constant gas flow rate of 60 ml/min was maintained, which was controlled by the gas flow controller "3" (Allicant Scientific, Tucson, AZ; Model MC-500SCCM-D, USA). X-ray powder diffraction (XRD; D8 Advance, AXS Corporation, Bruker, German, Cu Ka filtered radiation, and operated at 30 kV and 20 mA with a scanning speed of 10° min^{-1}) was used to identify the phase compositions. Morphologies of these samples were observed by the field-emission scanning electronic microscope (FE-SEM; Nova 400 NanoSEM, FEI Corporation, American, and with an acceleration voltage of 15 kV).

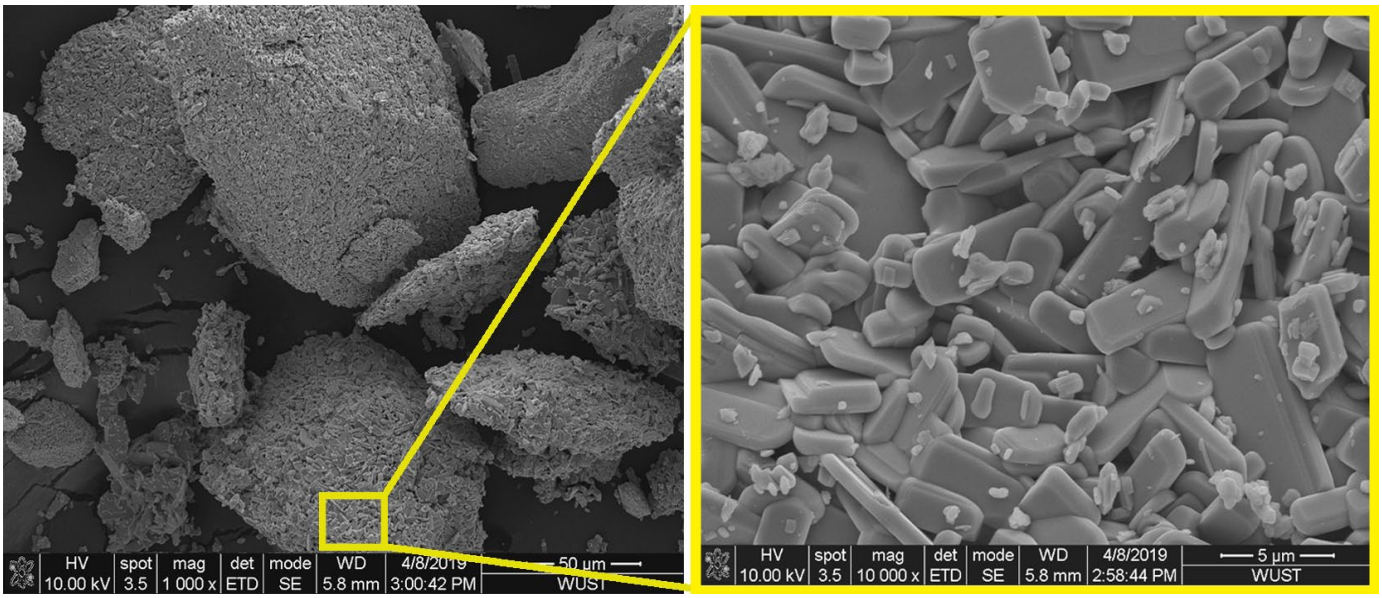

Fig. 2. Images of raw material MoO_3

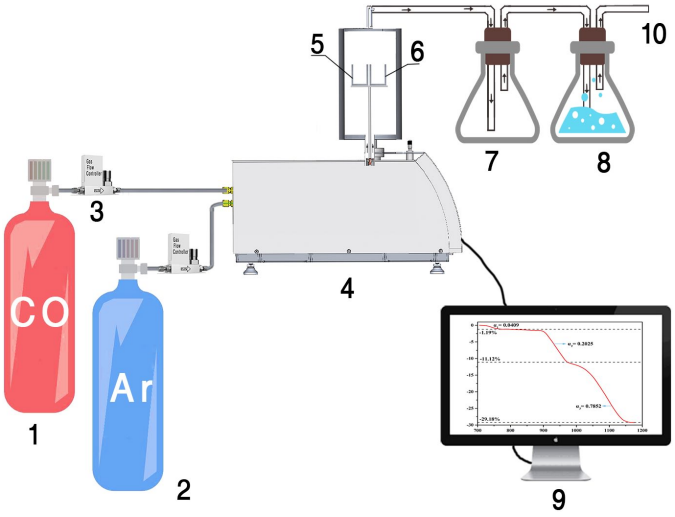

Fig. 3. Schematic diagram of the apparatus for the experiments: 1. CO gas; 2. Ar gas; 3. Gas flow controller; 4. HCT-3 TG analyzer; 5. Calibrated alumina crucible; 6. Experimental alumina crucible; 7. Beaker flask A; 8. Beaker flask B; 9. Data collector; 10. Exhaust gases

3. Result and discussion

3.1. Kinetics analyses

The reduction kinetics curves of samples doped with different contents of NaCl (0, 0.1, 0.5, and 2 wt.%) are shown in Fig. 4. It can be clearly seen that an obvious turning point appeared at the position of mass loss of 11.12% during the whole reaction processes, which is exactly equaled to the theoretical mass loss from MoO_3 to MoO_2, as shown in Eq. (1). The final mass loss is about 29.18%, which is also highly consistent with the theoretical value from MoO_3 to Mo_2C, as seen in Eq. (2). If considering the newly as-formed MoO_2 at the turning point as the reactant, then the second reaction was the reduction of MoO_2 to Mo_2C, as described in Eq. (3). From these results it can be concluded that the reaction processes of MoO_3 to Mo_2C were mainly proceeded in two steps, namely, the reduction of MoO_3 to MoO_2 and then the carburization of MoO_2 to Mo_2C. From the DTG curves shown in Fig. 4(B), it can be seen that even though the maximum reaction rate was decreased with the increase of NaCl additive (0.1, 0.5, and 2 wt.%), however, the time for maximum reaction rate became earlier at the first stage (mass loss from zero to 11.12%). As to the second stage, the maximum reaction was also decreased with increasing the content of NaCl except for 0.5 wt.% NaCl-doped samples.

$$MoO_3(s) + CO(g) = MoO_2(s) + CO_2(g) \quad (1)$$

$$2\,MoO_3(s) + 8\,CO(g) = Mo_2C(s) + 7\,CO_2(g) \quad (2)$$

$$2\,MoO_2(s) + 6\,CO(g) = Mo_2C(s) + 5\,CO_2(g) \quad (3)$$

In order to show the effect of different contents of NaCl on the reaction rate more intuitively, the mass losses curves of the first stage (from MoO_3 to MoO_2) and the second stage (from MoO_2 to Mo_2C) of the whole reaction processes as the function of reaction time were derived for the comparison convince, as shown in Fig. 5. In Fig. 5, the start reaction times for the reactions were determined as follows: due to the fact that the non-isothermal experiments were carried out under a constant heating rate (10 K/min), so the temperature was in direct proportion to the reaction time; as to the first stage ($MoO_3 \rightarrow MoO_2$), the starting reaction time can be counted from the starting reaction temperature. For example, 700 K can be considered as the starting reaction temperature for the 2 wt.% NaCl-doped MoO_3 samples, and then this position was counted as the initial reaction time, $t = 0$ min. The transformed results were shown in Fig. 5(A). In order to reflect the influence of NaCl on the second stage ($MoO_2 \rightarrow Mo_2C$) more intuitively, the starting point of the second stage was equaled to the end point of the first stage reaction (the position of the theoretical weight loss rate of 11.12%). For ease of comparison, the solid line represented the first stage, and the dashed line represented the second stage. Therefore, from Fig. 5(A) (except for the result of sample mixed with 2 wt.% NaCl) it can be obviously seen that the comprehensive reaction rate was increased with the increase of NaCl additive. As to the

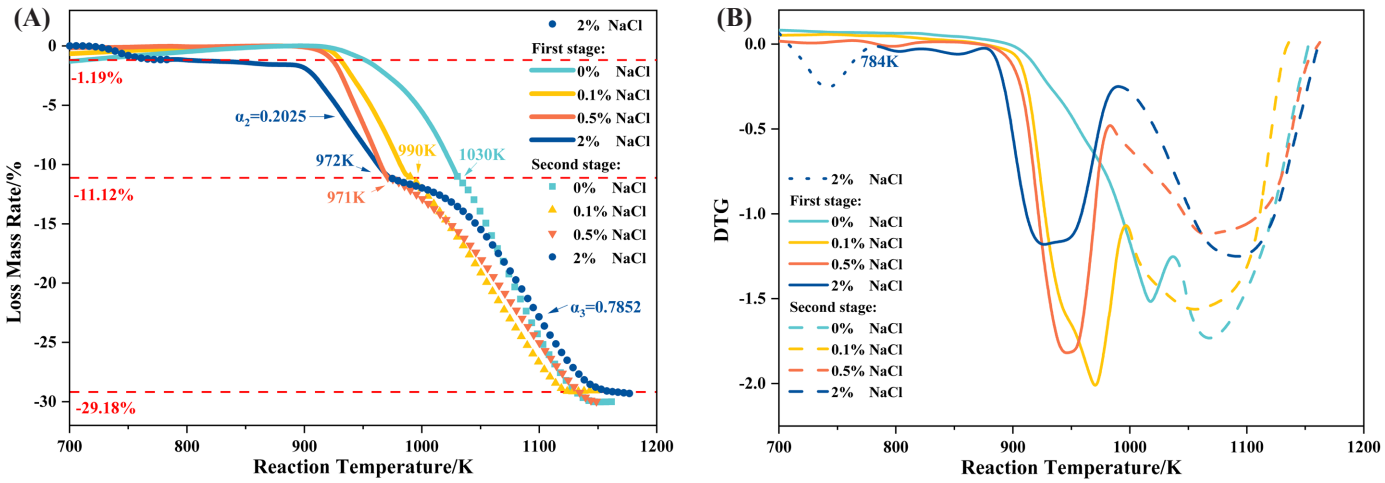

Fig. 4 The kinetics curves of samples mixed with different contents of NaCl (0, 0.1, 0.5, and 2 wt.%) reduced by high-purity CO gas: (A) TG curves; (B) DTG curves

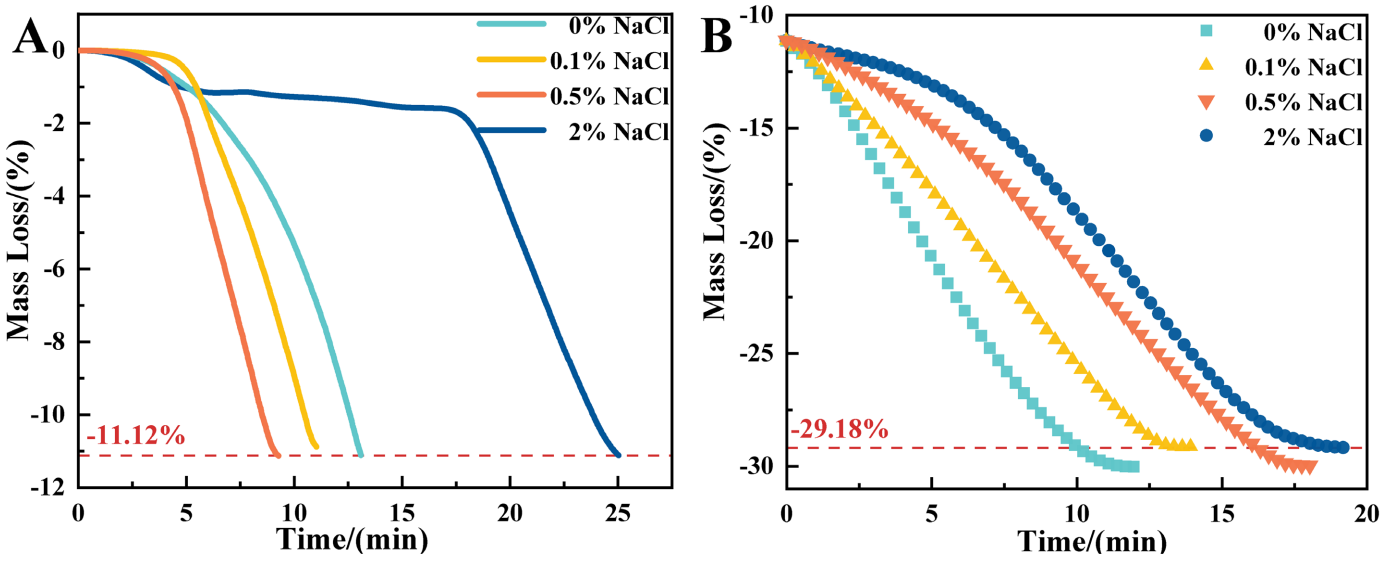

Fig. 5 Reduction kinetics curves of samples mixed with different contents of NaCl additive at: (A) the first stage; (B) the second stage

second stage, however, it can be found that the reaction behaviors were on the contrary, the larger the content of added NaCl was, the slower the reaction rate will be, as shown in Fig. 5(B).

As to the results obtained in the case of 2 wt.% NaCl-doped sample, the curve was quite different from those of 0, 0.1, and 0.5 wt.% NaCl-doped samples. There were three obvious turning points occurred during the whole reaction processes; the first stage was from the mass loss of 0 to 1.19%, which may be due to the formation of volatile molybdenum oxychoride ($MoO_2Cl_2(g)$), as shown in Eq. (4); the second stage was from 1.19% to 11.2% and third from 11.2% to 29.18%. Undoubtedly, MoO_2 and Mo_2C were successively formed at the second and third stages, respectively, which were the same as those obtained at 0, 0.1, and 0.5 wt.% NaCl-doped samples.

$$2\,MoO_3(s) + 2\,NaCl(s) = \\ = MoO_2Cl_2(g) + Na_2MoO_4(s) \qquad (4)$$

The reasons for the different kinetic curves can be explained as follows: due to the low boiling point and high sublimation property of $MoO_2Cl_2(g)$ [29-31], Eq. (4) was a mass loss reaction indeed. When the content of NaCl was 2 wt.%, the amount of newly as-formed $MoO_2Cl_2(g)$ was larger, so the mass loss would be obvious. However, when the added NaCl was very small (0.1 wt.% and 0.5 wt.%), the amount of newly as-formed $MoO_2Cl_2(g)$ was relatively small and even beyond the instrumental error; therefore, the mass loss caused by Eq. (4) can be ignored, and so the main mass loss shown in Fig. 4(A) is only reflected by the reduction of MoO_3 to MoO_2 at the first stage.

3.2. XRD analyses

The XRD patterns of the final products for the four samples (0, 0.1, 0.5, and 2 wt.% NaCl-doped MoO_3) were shown in Fig. 6. It was found that almost all the peaks were corresponded to Mo_2C, which indicated that the final product were mainly Mo_2C. Due to the fact that the added NaCl additive only occupied a very small amount, which was mainly used as the nucleating agent and the reaction of it with MoO_3 will also consume most of it, so the XRD technology could not detect it due to the very small amount. In other reference [27], NaCl was also used as the additive during the H_2 reduction process of MoO_2 to Mo, in which NaCl was also not detected in the product. That is to say, the small amount of NaCl has little effect on the final product under the current conditions.

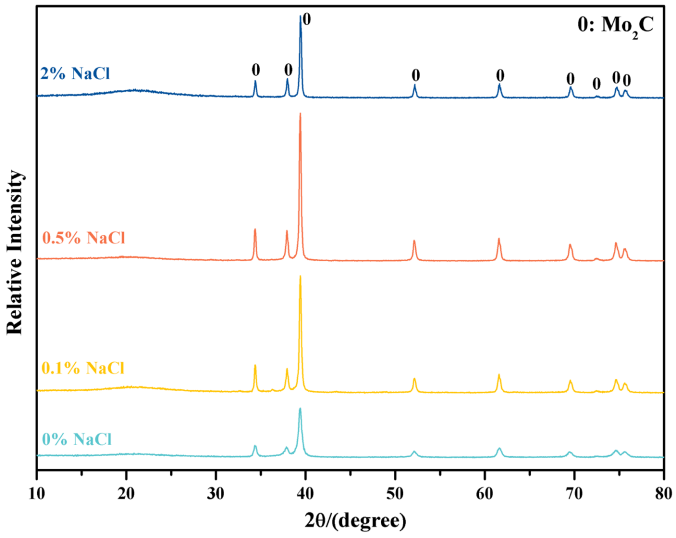

Fig. 6. XRD patterns of the reaction products obtained by reducing NaCl-doped MoO_3 samples with high-purity CO gas

The XRD patterns of reduction products for the 2 wt.% NaCl-doped samples at different reaction extents are presented in Fig. 7. It can be seen that a small amount of Na_2MoO_4 were formed during the first step of the reduction process, which will cover the surface of reactant and further hinder the reduction of MoO_3, that was why a flat was achieved during the lower temperature reaction stage, as shown in Figs. 4(A) and 5(A).

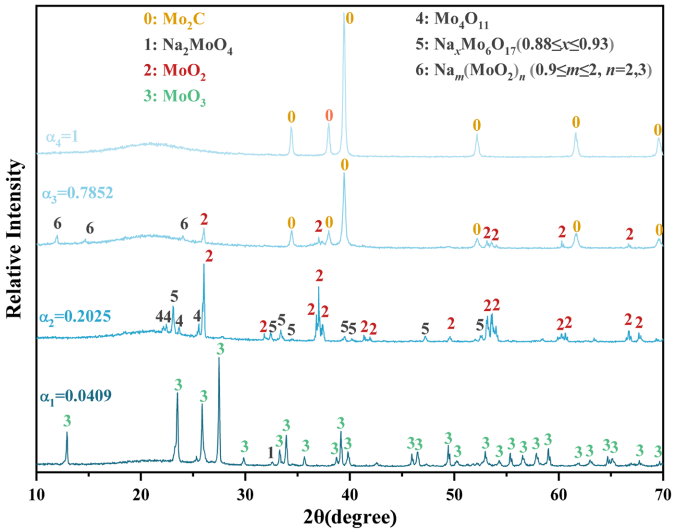

Fig. 7. XRD patterns of the reaction products obtained by reducing 2 wt.% NaCl-doped mixed MoO_3 with high-purity CO gas at different stages

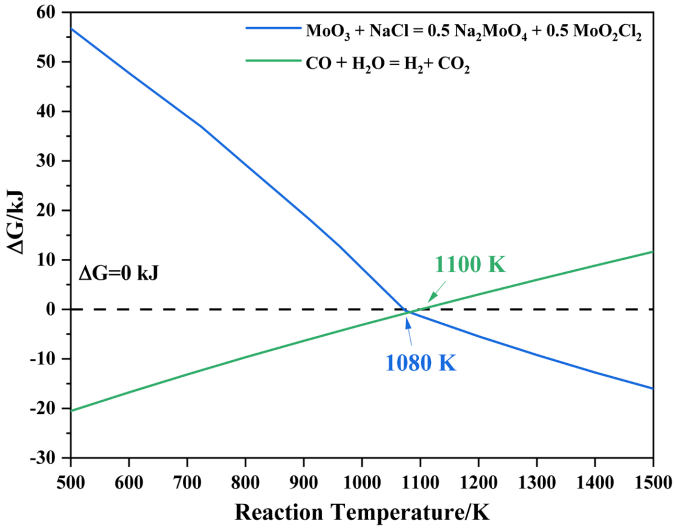

Fig. 8. The standard Gibbs free energy changes for Eqs. (4) and (9)

From the result it can be known that of MoO_3 and NaCl (seen Eq. (4)) could react with each other at a low temperature (700 K), which is much lower than the theoretical reaction temperature of 1080 K (seen Fig. 8). The lower reaction temperature may be due to the non-equilibrium state, similar results were also reported by Johnson et al. (703 K) [29], Aleksandrov et al. (723 K) [30] and Li et al. (823 K) [31]. When the reaction extent achieved 0.2025 (α = 0.2025), MoO_3 was mainly converted to MoO_2 and Mo_4O_{11}, as shown in Eqs. (5) and (6). Moreover, the low-melting-point eutectic $Na_xMo_6O_{17}$ ($0.88 \le x \le 0.93$) were also observed, which was mainly generated by the eutectic reaction of MoO_3 and Na_2MoO_4 [32]. When the reaction extent achieved 0.7852 (α = 0.7852), Mo_4O_{11} was disappeared and most of the MoO_2 was reduced to Mo_2C. Similarly, a small amount of low-melting-point eutectic $Na_m(MoO_2)_n$ were still existed. After the reaction completed, the products were almost composed of Mo_2C.

$$MoO_3(s) + 1/4\ CO(g) = 1/4\ Mo_4O_{11}(s) + 1/4\ CO_2(g) \quad (5)$$

$$1/4\ Mo_4O_{11}(s) + 3/4\ CO(g) = MoO_2(s) + 3/4\ CO_2(g) \quad (6)$$

3.3. FE-SEM for morphology observation

Fig. 9 presents the FE-SEM micrographs of the products obtained at different contents of NaCl additive. From Figs. 9(A1) and 9(A2), it can be obviously seen that morphology of Mo_2C powders obtained by reducing 0 wt.% NaCl-doped MoO_3 (pure MoO_3) powders are nearly maintained the original platelet-shaped morphology of MoO_3 raw material (Fig. 2) except for the porous surface, which may be due to the release of product gas. When adding a small amount of additives into MoO_3, the morphology of obtained product has a big change. For example, when the content of NaCl is 0.1 wt.%, some small pores are formed and the products keep regular platelet-shaped morphology with many small particles appeared on the surface, as shown in Figs. 9(B1) and 9(B2). When the content of NaCl increases to 0.5 wt.% or 2 wt.%, the morphology characteristic becomes denser and bigger, which may be due to the formation of liquid drops, and then sticking together with different particles, as shown in Figs. 9(C1) and 9(C2) as well as 9(D1) and 9(D2).

In order to observe the morphology evolution of the product during the reduction process, FE-SEM micrographs of 2 wt.% NaCl-doped samples at different reaction extents were also obtained and shown in Fig. 10. From Figs. 10(A1) to 10(A3) it can be observed that before the reaction began, the mixtures kept the same platelet-shaped morphology and smooth surface structure as the raw material. When the reaction extent was only 0.0409, some whiskers can be observed on the particles surface, which may be due to the deposited carbons produced by the carburization reaction (seen Eq. (7)), as shown in Figs. 10(B1) to 10(B3). Similar phenomenon was also reported in reference [33]. When the reaction extent reached 0.2025 (α = 0.2025), the products became bigger via the agglomerate effect with each other with keeping the same surface structure, as shown in Figs. 10(C1) to 10(C3). What is more, some low-melting-point eutectic (some complex compounds formed by the reaction between MoO_3 and Na_2MoO_4) began to form, which was in well agreement with the results of XRD pattern (seen Fig. 7). However, when the reaction extent was 0.7852 (α = 0.7852), the products became rough and filled of small pores, as shown in Figs. 10(D1) to 10(D3); after the reaction was completed (α = 1), these changes became more obvious, as shown in Figs. 10(E1) to 10(E3). During the whole reaction process, as the reaction proceeds forward, the products grew bigger and bigger as the adhesion become increasingly severe.

$$2\ CO = C + CO_2 \quad (7)$$

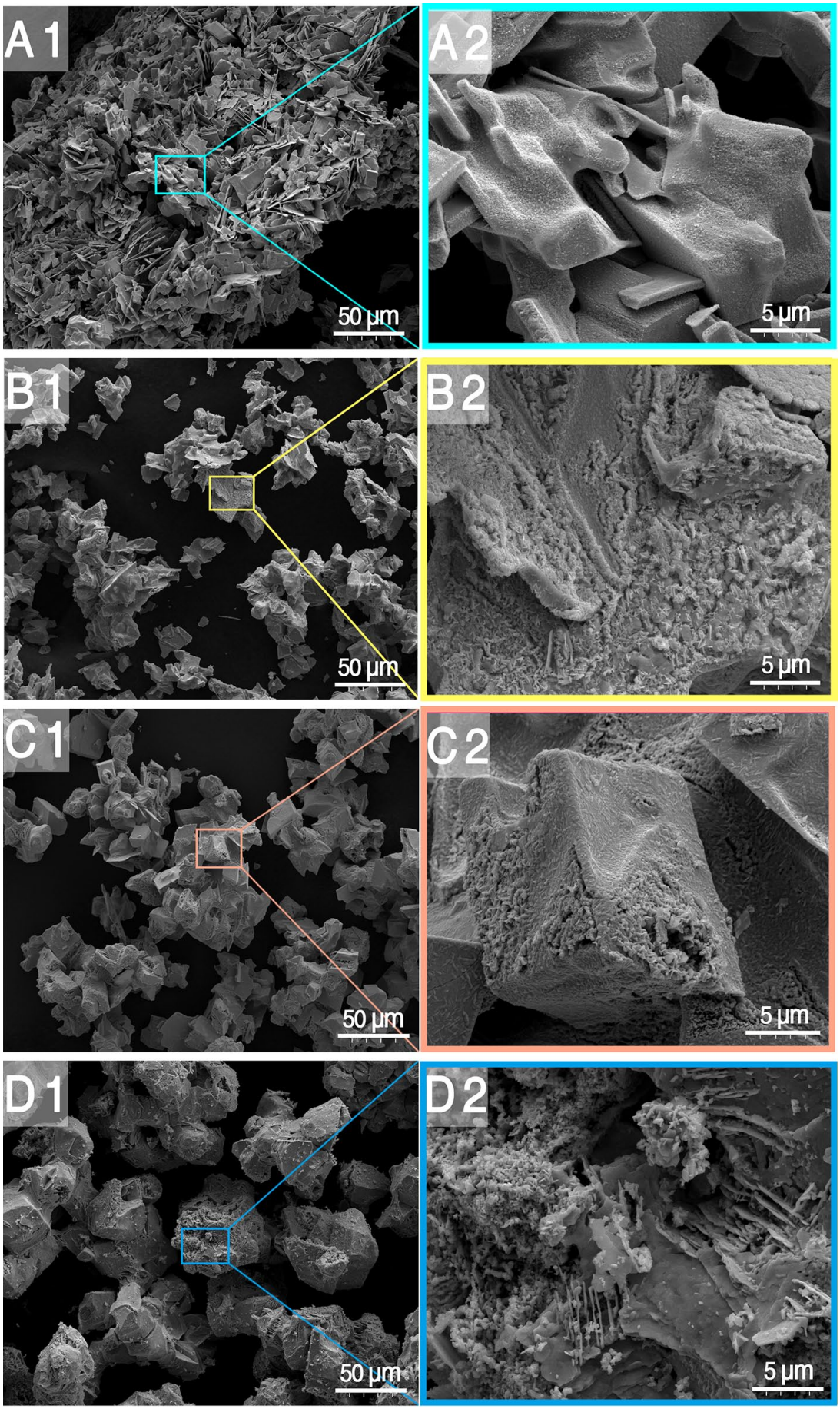

Fig. 9. A1-D2 FE-SEM micrographs of Mo_2C powders obtained by reducing NaCl-doped MoO_3. A1-A2: 0 wt.% NaCl-doped MoO_3; B1-B2: 0.1 wt.% NaCl-doped MoO_3; C1-C2: 0.5 wt.% NaCl-doped MoO_3; D1-D2: 2 wt.% NaCl-doped MoO_3

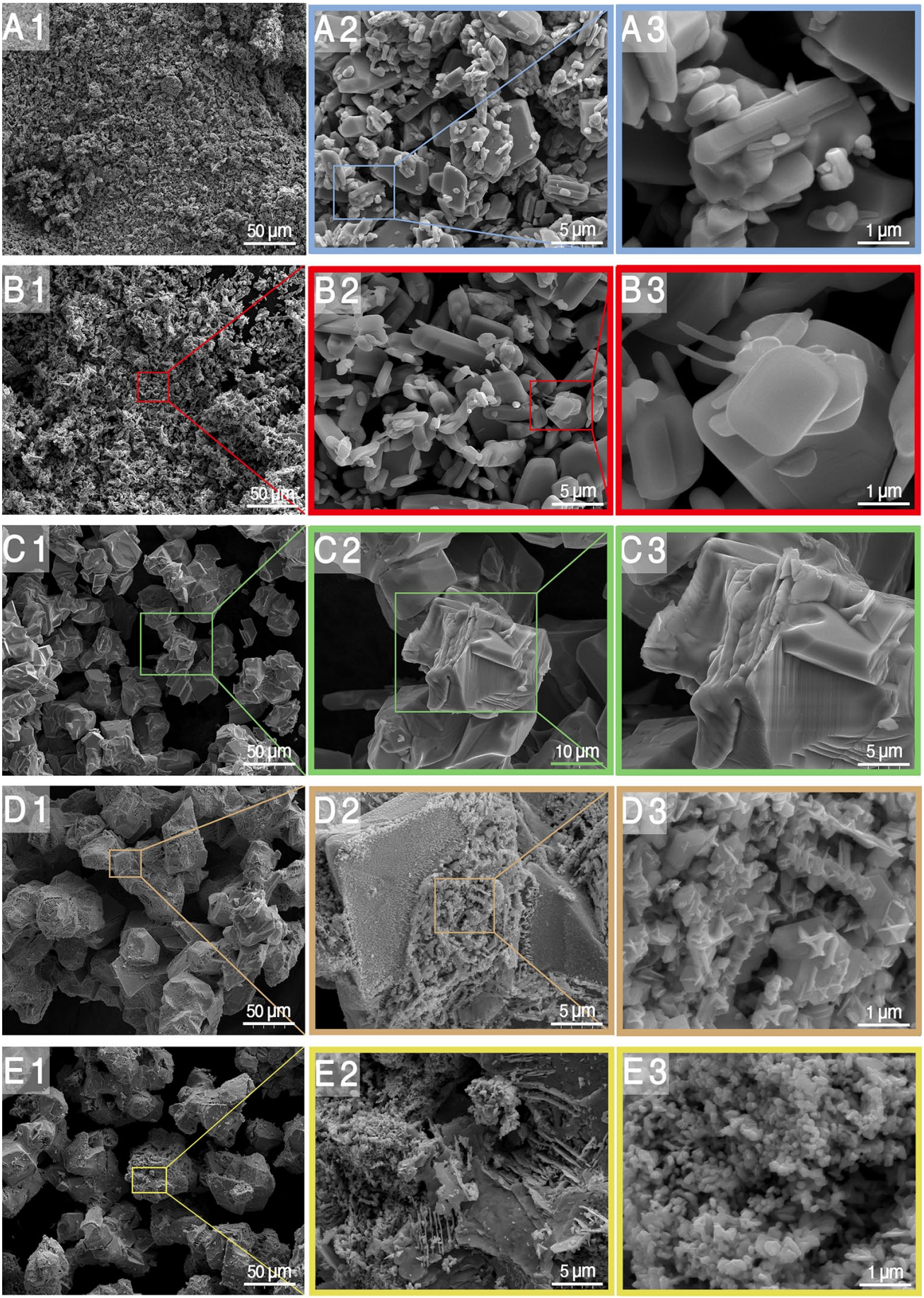

Fig. 10. FE-SEM micrographs of reaction products obtained by reducing 2 wt.% NaCl-doped mixtures at different reaction extents. A1-A3: $\alpha = 0$, B1-B3: $\alpha = 0.0409$, C1-C3: $\alpha = 0.2025$, D1-D3: $\alpha = 0.7852$; E1-E3: $\alpha = 1$

3.4. Reaction mechanism

As mentioned above, the reaction rate increases with the increasing content of NaCl (from 0 wt.% to 0.5 wt.%) at the first stage (from MoO_3 to MoO_2); however, at the second stage (from MoO_2 to Mo_2C), increasing the content of NaCl has a significant inhibitory effect. Therefore, it can be deduced that the reaction mechanisms between the two stages were different with each other during the reduction processes. Due to the adoption of spraying method for the preparation of mixed sample, a small amount of H_2O may still remain in the sample, which would lead to the formation of Mo-O-H compounds [34]. So, when the temperature increased to 700 K, Mo-O-H compounds and the volatilized MoO_2Cl_2 (as shown in Eq. (4)) gas may be co-existed and constructed the mixed Mo-O_x-Cl_y / Mo-O_m-H_n transport phases (TP) system, which would deposit on the nucleus of the product and accelerate the reaction or may be further reduced into the sub-oxides [35-37]. The difference between TP_1 and TP_2 lies in the atomic ratio of O/Cl or O/H. According to the characterizations of CVT [35] and current results, it can be inferred that the reduction reaction of the first stage may also obey the CVT mechanism, as shown in Eq. (8). Herein, something that should be noted is that even though reaction (9) may be existed (seen the thermodynamic result shown in Fig. 8) in the system, the proportion of it is very small, the main reductant is still CO gas, which could be verified by the final mass loss shown in Fig. 4, so the H_2 reduction process could be ignored. As shown in Eqs. (5) and (6), it is found that the reduction of MoO_3 to MoO_2 is a consecutive reaction with the formation of Mo_4O_{11} as the intermediate product, which was consistent with a larger number of literatures [38-40]. Due to the high vapor pressures of TP_1 and TP_2, more Mo_4O_{11} and MoO_2 cores will be formed, so larger numbers of small particles will be formed and grown into bigger platelet-shape particles, as shown in Fig. 11. Besides, due to the formation of low-melting-point eutectics (some complex compounds formed by the reaction between MoO_3 and Na_2MoO_4) [32] and the release of lots of heat produced by the exothermic reaction (Eq. (1) to Eq. (3), seen Fig. 12), the local temperature will be raised largely, which will further lead to the formation of agglomerative and make the particle become larger.

$$MoO_3 \rightarrow TP_1 \rightarrow Mo_4O_{11} \rightarrow TP_2 \rightarrow MoO_2 \quad (8)$$

$$CO(g) + H_2O(g) = H_2(g) + CO_2(g) \quad (9)$$

In addition, CO gas diffuses toward the reaction interface and undergoes a reduction reaction with MoO_2, after which the oxidation product CO_2 will diffuse through the product layers again. During the reaction process, 1 mol MoO_2 produced 0.5 mol Mo_2C, and thus the molar volume will decrease. The reasons are explained as follows: due to the fact that molar volume means the ratio of molar weight to the density; molar weights of 1 mol MoO_2 and 0.5 mol Mo_2C_5 were respective 127.94 g/mol and 101.94 g/mol, densities of them were respective 6.47 g/cm^3 and 9.18 g/cm^3, so the molar volumes of them could be easily calculated, i.e., 19.77 cm^3/mol and 11.1045 cm^3/mol, respectively. That is to say, molar volume of them had decreased from 19.77 cm^3/mol to 11.1045 cm^3/mol. Similar results were also reported in other literature [41]. Therefore, in order to maintain the same platelet-shaped morphology, the newly as-formed Mo_2C will produce many pores and cracks. Moreover, as the increase of NaCl additive, the adhesion of MoO_2 will be tighter

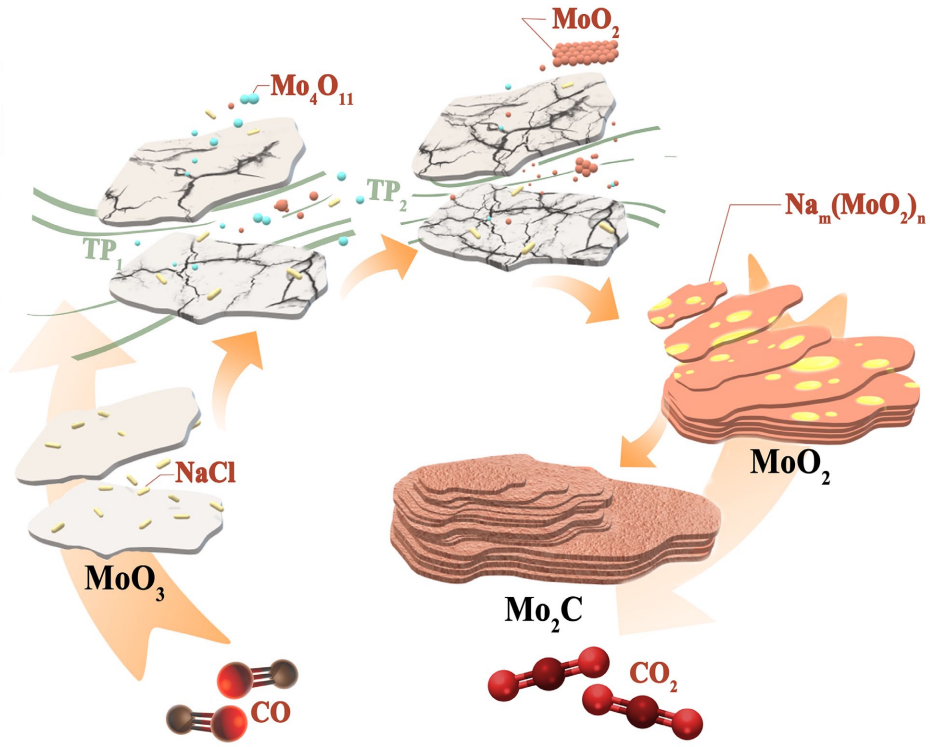

Fig. 11. Proposed possible mechanism diagram for the reduction reaction of NaCl-doped MoO_3 with high-purity CO gas

and the porosity will decrease accordingly, and so the reaction rate will be slowed down by limiting the diffusion rate of gaseous transport phase.

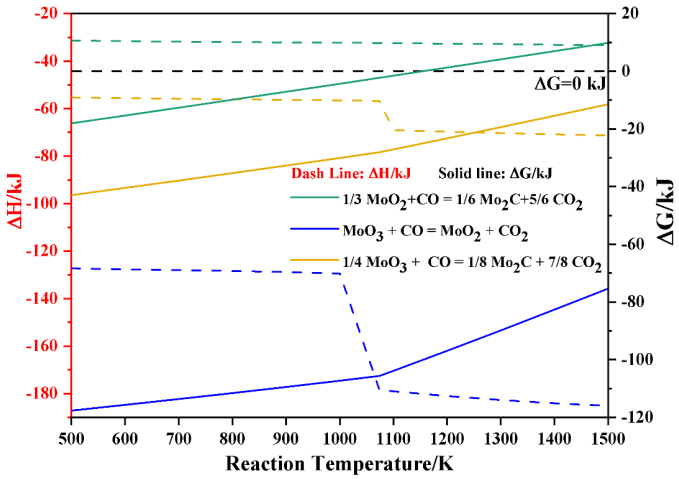

Fig. 12. The standard Gibbs free energy and enthalpy changes as the function of temperature for the reductions of MoO_3 with CO gas

4. Conclusions

This work studied on the influence of NaCl on the morphology and reduction rate during the reduction process of MoO_3 to Mo_2C under pure CO atmosphere. It was found that increasing the content of NaCl (from 0 wt.% to 0.5 wt.%) in MoO_3 could increase the reduction rate at the first stage (from MoO_3 to MoO_2) due to nucleation effect; while when the content of NaCl increased to 2 wt.%, the reaction rate will be inhibited. As to the second stage (from MoO_2 to Mo_2C), however, it was found the reaction rate will be decreased with the increase of NaCl additive due to the formation of low-melting-point eutectic. Particle size of Mo_2C was gradually increased with the proceeds of the reaction and the increase of added NaCl additives, the corresponding reaction mechanisms were proposed.

Acknowledgments

The authors gratefully acknowledge the financial support from the Guangdong Province Basic and Applied Basic Research Foundation (2019A1515110361), and the Special Project of Central Government for Local Science and Technology Development of Hubei Province (2019ZYYD076).

REFERENCE

[1] F.X. Ma, B.H. Wu, B.Y. Xia, C.Y. Xu, X.W. Lou, Angew. Chem., Int. Ed. **54** (51), 15395-15399 (2015).

[2] E.J. Pavlina, J.G. Speer, C.J. Van Tyne, Scripta Mater. **66** (5), 243-246 (2012).

[3] N. Perret, X. Wang, L. Delannoy, C. Potvin, C. Louis, M.A. Keane, J. Catal. **286**, 172-183 (2012).

[4] Y. Chen, S. Choi, L.T. Thompson, J. Catal. **343**, 147-156 (2016).

[5] H. Wang, S. Liu, K.J. Smith, J. Catal. **369**, 427-439 (2019).

[6] S. Liu, H. Wang, K.J. Smith, C.S. Kim, Energ. Fuel **31** (6), 6378-6388 (2017).

[7] J.C. Schlatter, S.T. Oyama, J.E. Metcalfe III, J.M. Lambert Jr, Ind. Eng. Chem. Res. **27** (9), 1648-1653 (1988).

[8] A. Szymańska-Kolasa, M. Lewandowski, C. Sayag, D. Brodzki, G. Djéga-Mariadassou, Catal. Today. **119** (1-4), 35-38 (2007).

[9] T.C. Xiao, A.P. York, H. Al-Megren, C.V. Williams, H.T. Wang, M.L. Green, J. Catal. **202** (1), 100-109 (2001).

[10] L. Wang, Z.L. Xue, A. Huang, F.F. Wang, ACS Omega. **4** (22), 20036-20047 (2019).

[11] L. Wang, G.H. Zhang, K.C. Chou, J. Aust. Ceram. Soc. **54** (1), 97-107 (2018).

[12] Z. Lv, J. Dang, Y. Wu, X. Lv, S. Zhang, J. Mater. Sci. **53** (14), 10059-10070 (2018).

[13] J. Dang, G. Zhang, L. Wang, K. Chou, P.C. Pistorius, J. Am. Ceram. Soc. **99** (3), 819-824 (2016).

[14] J.A. Nelson, M.J. Wagner, Chem. Mater. **14** (4), 1639-1642 (2002).

[15] T. Hyeon, M. Fang, K.S. Suslick, J. Am. Chem. Soc. **118** (23), 5492-5493 (1996).

[16] X. Liu, N Fechler, M. Antonietti, Chem. Soc. Rev. **42** (21), 8237-65 (2013).

[17] L. Zhu, Q. Huang, Ceram. Int. **3 7**(1), 239-255 (2011).

[18] X. Chen, Y. Li, Y. Li, J. Zhu, S. Jin, L. Zhao, Z. Lei, X. Hong, Ceram. Int. **34** (5), 1253-1259 (2008).

[19] X. Liu, C. Gioradno, M. Antonietti, Chem. Mater. **25** (10), 2021-2027 (2013).

[20] N. Fechler, T.P. Fellinger, M. Antonietti, Adv. Mater. **25** (1), 75-79 (2013).

[21] W. Han, K. Liu, S. Yang, F. Wang. J. Su. B. Jin. H. Li, T. Zhai, Sci. China Chem. **62** (10), 1300-1311 (2019).

[22] J. Zhou, J. Lin, X. Huang, Y. Zhou, Y. Chen, J. Xia, H. Wang, Y. Xie, H. Yu, J. Lei, D. Wu, F. Liu, Q. Fu, Q. Zeng, C. Hsu, C. Yang, L. Lu, T. Yu, Z. Shen, H. Lin, B.I. Yakobson, Q. Liu, K. Suenaga, G. Liu, Z. Liu, Nature **556** (7701), 355-359 (2018).

[23] X. Hu, P. Huang, B. Jin, X. Zhang, H. Li, X. Zhou, T. Zhai, J. Am. Chem. Soc. **140** (40), 12909-12914 (2018).

[24] C. Lan, Z. Zhou, R. Wei, J.C. Ho, Mater. Today Energy **11**, 61-82 (2019).

[25] Z. Zhang, P. Chen, X. Duan, K. Zang, J. Luo, X. Duan, Science. **357** (6353), 788-792 (2017).

[26] G.H. Zhang, J.J. Li, L. Wang, K.C. Chou, Int. J. Refract. Met. H. **69**, 180-188 (2017).

[27] G.D. Sun, G.H. Zhang, S.Q. Jiao, K.C. Chou, J. Phys. Chem. C. **122** (18), 10231-10239 (2018).

[28] G.D. Sun, G.H. Zhang, K.C. Chou, Int. J. Refract. Met. H. **78**, 68-75 (2019).

[29] D.A. Johnson, J.H. Levy, J.C. Taylor, A.B. Waugh, J. Brough, Polyhedron. **1** (5), 479-482 (1982)

[30] P.V. Aleksandrov, A.S. Medvedev, M.F. Milovanov, V.A. Imideev, S.A. Kotova, D.O. Moskovskikh, Int. J. Miner. Process. **161**, 13-20 (2017).

[31] S. Li, Y.C. Lin, W. Zhao, J. Wu, Z. Wang, Z. Hu, Y. Shen, D.M. Tang, J. Wang, Q. Zhang, H. Zhu, Nat. Mater. **17** (6), 535-542 (2018).

[32] Y.G. Petrosyan, V.M. Zhukovskii, O.A. Ustinov, T.M. Panfilova. Zh. Neorg. Khim. **22** (10), 2841-2844 (1977).

[33] L. Wang, C.Y. Bu, G.H. Zhang, J.S. Wang, K.C. Chou, Metall. Mater. Trans. B. **48** (4), 2047-2056 (2017).

[34] G.D. Sun, G.H. Zhang, X.P. Ji, J.K. Liu, H. Zhang, K.C. Chou, Int. J. Refract. Met. H. **80**, 11-22 (2019).

[35] W.V. Schulmeyer, H.M. Ortner, Int. J. Refract. Met. H. **20** (4), 261-269 (2002).

[36] J. Dang, G H. Zhang, K.C. Chou, R.G. Reddy, Y. He, Y. Sun, Int. J. Refract. Met. H. **41**, 216-223 (2013).

[37] J. Dang, G.H. Zhang, K.C. Chou, High Temp. Mater. Proc. **33** (4), 305-312 (2014).

[38] R. Burch, J. Chem. Soc., Faraday Trans. 1. **74**, 2982 (1978).

[39] T. Leisegang, A.A. Levin, J. Walter, D.C. Meyer, Cryst. Res. Technol. **40** (1-2), 95-105 (2005).

[40] L. Wang, G.H. Zhang, K.C. Chou, Int. J. Refract. Met. H. **54**, 342-350 (2016).

[41] L. Wang, G.H. Zhang, K.C. Chou, J. Aust. Ceram. Soc. **54** (1), 97-107 (2018).